Liquid Crystals
Publication details, including instructions for authors and subscription information:
http://www.informaworld.com/smpp/title~content=t713926090

Structural aspects of the nematic-isotropic transition in liquid crystals: an investigation using a development of the Lebwohl-Lasher lattice model

Dominique Gonin; Alan Windle

Online publication date: 11 November 2010

To cite this Article Gonin, Dominique and Windle, Alan(1997) 'Structural aspects of the nematic-isotropic transition in liquid crystals: an investigation using a development of the Lebwohl-Lasher lattice model', Liquid Crystals, 23: 4, 489 — 502
To link to this Article: DOI: 10.1080/026782997208073
URL: http://dx.doi.org/10.1080/026782997208073

LIQUID CRYSTALS, 1997, VOL. 23, NO. 4, 489–502

Structural aspects of the nematic–isotropic transition in liquid crystals: an investigation using a development of the Lebwohl–Lasher lattice model

by DOMINIQUE GONIN
PCSM, ESPCI, 10 rue Vauquelin, 75231 Paris Cedex 05, France

and ALAN WINDLE*
Department of Materials Science and Metallurgy, Cambridge University, Pembroke St., Cambridge CB2 3QZ, UK

(*Received 13 January 1997; in final form 1 June 1997; accepted 13 June 1997*)

This paper explores further the predictions of the Lebwohl–Lasher model [1] for the description of order in a liquid crystalline system, especially in the region of the nematic–isotropic transition. The model is based on a lattice, each cell of which contains a director representing the long axis of a rod molecule. The energy of each director is determined by the relative orientations of its six nearest neighbours, and the probability of a director orientation being moved to another chosen at random depends on the Boltzmann function of the difference between the old and the new energies in accord with the normal Monte Carlo procedure. The validity of this model to describe this transition has been demonstrated in several previous studies [2–16] and its simplicity permits calculations over a statistically significant number of molecules.

Preliminary studies of the model behaviour have been made below the transition temperature in order to investigate the influence of boundary conditions. The simulated $\langle P_2 \rangle$ and $\langle P_2 \rangle / \langle P_4 \rangle$ quantities are compared both with experimental data and with the theory of Maier and Saupe [17]. The predictions of the model are analysed in the normal way using the Ornstein–Zernike expression for pairwise correlation functions, while this expression is modified in order to describe the short-range order which is superimposed on the background level of long-range order present in the nematic phase. The model's predictions of enthalpy changes across the transition are compared with calorimetric data from the literature [18]. The opportunity of working with a large model is taken to extend the Zhang plot to test for the presence of first order character within the transition.

A structural description of the transition is proposed, based on the molecular director maps, and the identification of more ordered and less ordered regions achieved by the analysis of the distribution of local energies into two sub-distributions with widths in accord with the mean values of their energies. As the transition is approached from above, the isotropic melt structure is seen to contain nematic nuclei which increase in volume fraction with decreasing temperature. At the transition these nuclei appear to join to give a percolating phase having a single orientation across the model. With decreasing temperature within the nematic region, isolated regions of disorder become continually smaller with a corresponding increase in the overall order parameter (P_2).

This paper focuses particularly on the structural implications of the predicted nematic–isotropic transition. It is recognized that aspects characterizing the physics of the transition can be obtained through averaging energy parameters over very large numbers of cycles, and using models as large as possible. While the 50^3 model presented here is particularly large by current standards, it is designed in this way to show a representative picture of the structure in the transition region. The aspect of the work reported, despite the availability of a large model, does not seek to generate better averages than previously reported, and the calculation of some such parameters in the earlier sections is to check that the model is behaving properly and in accord with results reported previously.

*Author for correspondence.

0267–8292/97 $12·00

1. Introduction

The magnitude of the scalar order parameter Q in the nematic phase and its evolution with temperature can be predicted by molecular field theories. These theories are based on the mean field approximation [17], and consequently do not given any information concerning short-range orientational correlations. Furthermore, it appears that in the nematic phase, a few degrees below the transition, a correct fit to and interpretation of experimental data become rather difficult [19, 20], and the values of Q calculated from the mean field approach are an over-estimate. This shortcoming is likely to be associated with the fact that short-range order is modelled only poorly by mean field theories while at these temperatures local fluctuations in the degree of order in the nematic occur. A corollary of this conjecture is the experimental evidence of short-range order just above the transition temperature, well-known as 'pre-transitional effects'. Indeed, de Gennes extended the Landau theory to the description of these phenomena, describing the true isotropic state as a uniform system devoid of nematic droplets, or 'swarms' [21–23].

Pre-transitional effects occur in the isotropic phase as the temperature reduces towards the nematic–isotropic transition temperature T_{NI}. Even though there is no long range order in this temperature range (the macroscopic order parameter having vanished discontinuously at T_{NI} on heating), the material still shows evidence of local order. The liquid has an inhomogeneous distribution of free energy density at any instant in time, and disconnected nematic nuclei are associated with the lower energy regions [23], the absence of orientational correlation from one swarm to another being consistent with the absence of long-range order. The average size of these regions of short-range order is given by the characteristic distance $\xi(T)$, called the coherence length.

Close to the transition, the thermodynamic behaviour of the material is usually described by the well-known Landau–de Gennes (LDG) theory [21–25]. The density of free energy is expanded in powers of the tensor order parameters. For a uniaxial nematic phase, this tensor expressed through the director components has a very simple matrix form:

$$[Q] = \begin{bmatrix} -Q/2 & & \\ & -Q/2 & \\ & & Q \end{bmatrix} \tag{1}$$

and the expansion of the free energy in terms of order parameter modulus is then:

$$F = F_i + \frac{1}{2}AQ^2 - \frac{1}{3}BQ^3 + \frac{1}{4}CQ^4 + \ldots \tag{2}$$

with F_i the free energy density in the isotropic phase. The B and C coefficients are only weakly temperature dependent close to the transition, and B characterizes the strength of the first order character of the transition. If the series is truncated after the Q^4 term, the order parameter at the transition point has the simple form:

$$Q_{NI} = 2B/3C. \tag{3}$$

The A coefficient changes sign according to:

$$A = a(T - T^*) \tag{4}$$

where T^* ($T^* < T_{NI}$) is the temperature at which the isotropic phase is totally unstable. The absolute stability limit of the nematic phase T^{**} ($T^{**} > T_{NI}$) can also be defined, and the order parameters at T^* and T^{**} are, respectively:

$$Q^* = B/C \tag{5}$$

$$Q^{**} = B/2C. \tag{6}$$

In the nematic phase, the temperature dependence of the order parameter can be fitted with the formula:

$$Q = Q^{**} + k(T^{**} - T)^{\beta} \tag{7}$$

where $\beta = 0{\cdot}5$ where equation (2) is truncated.

A simple static description of the nematic–isotropic transition cannot be totally satisfactory, since order parameter modulus fluctuations can strongly influence the thermodynamic behaviour at the transition. De Gennes succeeded in accounting for the fluctuations by adding spatial derivatives to the expansion by means of the continuum theory:

$$F = F_i + \ldots + \frac{1}{2}L_1\left(\frac{\partial}{\partial x_i}Q_{jk}\right)^2 + \frac{1}{2}L_2\left(\frac{\partial}{\partial x_j}Q_{jk}\right)^2 \tag{8}$$

with L_1 and L_2 the elastic constants in the isotropic phase. This generalized Landau–de Gennes (GLDG) theory leads to a better description of the nematic nuclei, without abrupt changes in orientation at their borders. The response functions are defined in terms of correlation functions, and the temperature dependence of the correlation length is found to be:

$$\xi = \xi_0\left(\frac{T^*}{T - T^*}\right)^{1/2} \tag{9}$$

where ξ_0 has molecular dimensions. The analysis of the correlation functions in the Orstein–Zernike approximation predicts the spatial correlation of the order parameter to have the form:

$$\langle Q(0)Q(R)\rangle = \frac{\text{const}}{R}\exp(-R/\xi). \tag{10}$$

2. Simulations

2.1. *Lebwohl–Lasher model*

The Lebwohl–Lasher (LL) model is a simplified representation of the nematic liquid crystal, since the centres of gravity of the mesogenic units are confined to the sites of a cubic lattice. The molecules are free to rotate to minimize their interaction energy with their nearest neighbours, but there is no possible coupling between position and orientation. The Hamiltonian is derived from the Maier–Saupe attractive anisotropic interaction pair-potential:

$$H_{\mathrm{LL}} = -\varepsilon \sum_{\langle i,j \rangle} P_2(\cos\theta_{ij}) \tag{11}$$

where the sum is over all pairs of nearest neighbours, ε is a positive constant, and θ_{ij} is the angle between the long axes of the two neighbouring molecules.

However, despite its simplicity the model is extremely effective in predicting the order parameter right up to the nematic–isotropic transition, and it has been widely used, especially with the Monte Carlo method. Terms can be added to the Hamiltonian to get a better description for real materials [12, 14], or to study different systems such as ferroelectrics [26, 27]. The model, in its most simple form, has been shown to provide all the important characteristics of the nematic–isotropic phase transition, in accordance with experiment. The precision of the prediction of the order of the transition and its temperature is, as ever, limited by the finite size of the model used.

A better estimate of the precise transition temperature and associated parameters, as well as a more precise study of pre-transitional effects has been achieved either by correlation function analysis [6, 16] or by using [12] the Ferrenberg–Swendsen re-weighting technique [28] combined with Lee–Kosterlitz finite size scaling analysis [11]. The latter authors have shown the validity of the finite-size scaling relation:

$$\Delta T \ (\equiv T_{\mathrm{NI}} - T_{\mathrm{NI}}(L)) = \mathrm{const}\,(L^d)^{-1} \tag{12}$$

$L^d = N$ being the lattice size. Hence for the system size of 16^3, a constant of $(15{\cdot}6 \pm 8{\cdot}2)\varepsilon/k_{\mathrm{B}}$, k_{B} being the Boltzmann factor, and a transition temperature of $1{\cdot}1232\varepsilon/k_{\mathrm{B}} = 298\,\mathrm{K}$, the calculated transition temperature would be within $1 \pm 0{\cdot}53$ degrees above the true value. The LL approach, in the latter case, has also provided evidence for the first order character of the nematic–isotropic transition. Indeed, a 'double-well' distribution of the free energy as a function of nematic order has been shown, although in a very small temperature range around the transition [12].

2.2. *The application of the Lebwohl–Lasher model to this study*

The Hamiltonian is written in the form:

$$H = A \sum_{\langle i,j \rangle} \sin^2\theta_{ij} = H_{\mathrm{LL}} + \frac{2}{3}A \tag{13}$$

with $A = (3/2)\varepsilon$ and the summation limited to neighbouring cells. Expressed in this way, the Hamiltonian links to previous work in which microstructure was modelled at the meso-level [29], where the $\sin^2\theta$ function proved a good approximation to the dependence of elastic distortion energy on director misalignment as described by continuum theory. For a given distortion of the nematic field, the energy of a volume (l^3) scales as kl in the continuum case, where k is the unified elastic constant from Frank's equation (splay = twist = bend). The value of the constant A can thus be assessed for the cell of edge length equal to molecular dimensions used in the LL model, a, as ka. The value of k is known experimentally to be in the range $0{\cdot}5$–$1{\cdot}0 \times 10^{-11}\,\mathrm{J\,m^{-1}}$ for small molecule liquid crystals, and 'a' is of the order of 1 nm. Hence A is in the range $0{\cdot}5 \times 10^{-20}$–$1{\cdot}0 \times 10^{-20}\,\mathrm{J}$. The approximation that $A = 10^{-20}\,\mathrm{J}$ leads to predictions of the nematic–isotropic transition temperature in the range $400 \pm 125\,\mathrm{K}$, in general accord with real materials.

The calculations have been performed on 50^3 cubic lattices with periodic boundary conditions. This size of lattice, while being the maximum practicable with the resources available, should enable $T_{\mathrm{NI}}(50)$ to be very close to T_{NI} as indicated by equation (12): $T_{\mathrm{NI}}(50) = T_{\mathrm{NI}}(\infty) + 0{\cdot}033\,\mathrm{K}$ for a material with a 298 K N–I transition. The Metropolis Monte Carlo algorithm has been applied to obtain the thermodynamical equilibrium configurations, with a slight modification in that the new configurations are retained with a probability p:

$$p = \frac{\exp(-\Delta E/kT)}{1 + \exp(-\Delta E/kT)} \tag{14}$$

with $\Delta E = E_{\mathrm{new}} - E_{\mathrm{old}}$. The probability is 0·5 if the two energies are equal, and tends quickly to 1 as E_{new} decreases with respect to E_{old}. The description is thus more realistic for a model based on molecular scale entities, where the continuum practice of taking p to be equal to 1, whenever E_{new} becomes lower than E_{old}, is less appropriate, especially when ΔE is small.

The equilibrium is considered to be reached when the same level of average global order is obtained for models started, in turn, from a perfectly ordered system and from a totally disordered system. The various averages are then calculated over 1200, 2400 or 12 000 cycles, depending on the stability of the calculated parameter

at a given temperature, where a cycle corresponds to one visit per cell, or 50^3 visits over the model as a whole.

The nematic order parameter is defined as:

$$\langle P_2 \rangle = \left\langle \frac{3\cos^2\theta - 1}{2} \right\rangle_N \qquad (15)$$

where θ is the angle between a given molecular axis and the nematic director. The director orientation is found using an algorithm which searches for the unit vector direction which gives the maximum value of $\langle P_2 \rangle$ for a given configuration. The $\langle P_2 \rangle$ values are sampled at regular intervals of time once the model has reached equilibrium, and the best value taken as the temporal average.

Another parameter computed as the model average is the mean of the local interaction energies $\langle E_{\text{local}} \rangle$ which can be expressed as:

$$\langle E_{\text{local}} \rangle = \frac{A}{N} \left\langle \sum_{\langle i,j \rangle} \sin^2 \theta_{ij} \right\rangle . \qquad (16)$$

The probability distribution of the local energy, $P(E_{\text{local}})$, is given by the summation over each cell and its nearest neighbours, built up using all the model cells, over the run time of the model after an equilibrium state has developed from the start up configuration.

To evaluate short-range order, the angular pair correlation coefficient [6, 7] $G_2(r_{12}) = \langle P_2(\cos\theta_{12}) \rangle$ has also been calculated, where θ_{12} is the angle between the molecules of cells 1 and 2. This coefficient gives the correlation between the orientations of two particles separated by any distance r_{12}, up to the limits imposed by model size. It is then a measure of short-range order for small values of r_{12}, and tends to the nematic order parameter squared $\langle P_2 \rangle^2$ when r_{12} tends to infinity [30]. The $G_2(r_{12})$ decay above the transition temperature can be fitted with an Ornstein–Zernike form [6].

3. Determination of order parameters from the model

3.1. *Influence of the boundary conditions*

Periodic boundary conditions are usually applied in lattice modelling in order to simulate an infinite system, putting the lattice in a self-similar environment. The concern over periodic boundary conditions stems from their possible contribution to long range order, in that orientational information from one extremity of the model is translated to the other side. As a comparison, 'energy compensated free boundary' conditions were also investigated. In this case, the state of orientation is not copied from one side of the array to the other side, and the orientation of the directors in the border cells is left free, although in order to avoid melting due to surface effects, the border cell energies are rescaled with a factor which compensates for the missing nearest neighbours—one for a face, two for an edge and so on.

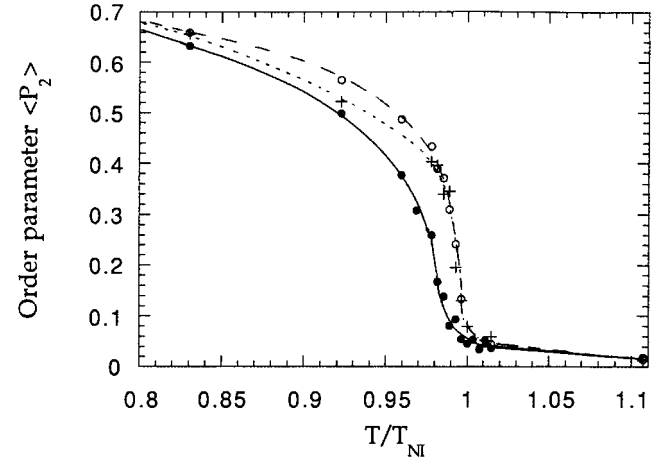

Figure 1. Plots of the order parameter as determined from the LL model for a 20^3 model against reduced temperature for different boundary conditions. Compensated free boundary conditions (full circles); periodic boundary conditions (open circles); data from a 20^3 model embedded in a 50^3 model (crosses).

The temperature dependence of $\langle P_2 \rangle$ has been calculated with a 20^3 lattice with the two different boundary conditions, and compared with a reference, obtained by examination of a 20^3 central region embedded in a 50^3 lattice with periodic boundary conditions. The results in figure 1 show good agreement between the reference and the periodic boundary conditions in close proximity to the transition, although there is some indication that the order for the periodic boundaries at temperatures less than 0·95 is rather higher than the reference. The fact that the order does not drop instantly to zero at the transition is associated with the presence of short-range order nematic nuclei of dimensions approaching that of the model (20^3). The 'print through' of the order within the nematic nuclei onto the $\langle P_2 \rangle$ versus temperature plot above the transition will be reduced for the larger models (look ahead to figure 2 (closed circles)), and would of course be absent for an infinite model. The energy compensated free boundaries gave rise to a P_2 versus temperature relationship which nevertheless appears to show residual free boundary effects. This approach has not been pursued further.

In the work which follows, all the calculations have been done with periodic boundary conditions.

3.2. *Quantification of long-range and short-range order*

Results obtained for the temperature dependence of the order parameter are comparable to previous reports for smaller lattices, except above the transition, where the residual global order parameter due to finite model

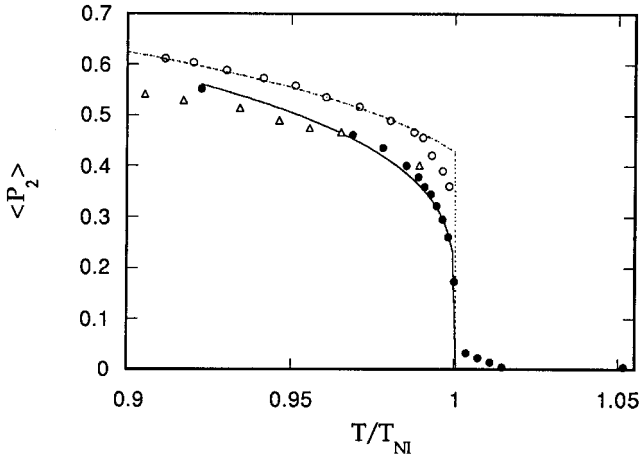

Figure 2. Plot of the order parameter against temperature for a 50^3 model with periodic boundary conditions (full circles) fitted with equation (7) with the β parameter = 0·32 (solid line). The dotted line is the Maier–Saupe prediction, while the open triangles are for experimental data for PAA at constant volume [20], and the open circles data for the same material at constant pressure [31].

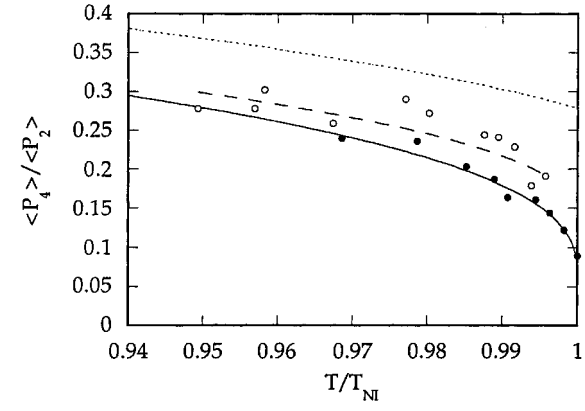

Figure 3. Temperature dependence of the ratio $\langle P_4\rangle/\langle P_2\rangle$ calculated from the 50^3 model (closed circles fitted with the solid line). The model data are compared with the Maier–Saupe prediction (dotted curve) and with experimental points measured at constant pressure by Kohli *et al.* [32] (open circles and dashed line).

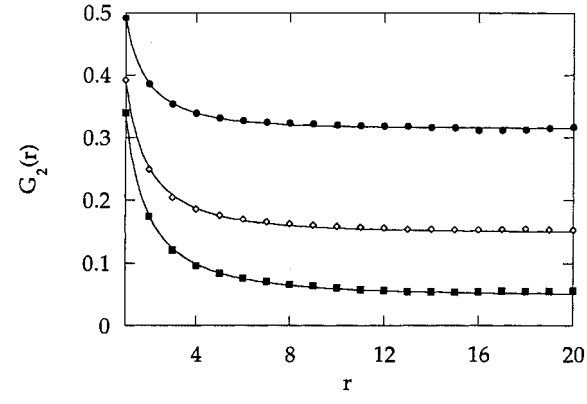

Figure 4. Fit of the angular pair correlation coefficients determined from the model to equation (17): at $T/T_{NI} = 0{\cdot}922$, with $\xi = 4{\cdot}9$ (full circles); at $T/T_{NI} = 0{\cdot}985$, with $\xi = 6{\cdot}4$ (open diamonds); at $T/T_{NI} = 1$, with $\xi = 7{\cdot}8$ (full squares).

size is predictably smaller (see figure 2). The quantitative values of $\langle P_2\rangle$ below the transition temperature are in good agreement with experimental data measured at constant volume for the rigid molecule PAA [20]. Such experimental data are not available close to the transition, but it can be seen that the shape of the curve is similar to the experimental curves measured at constant pressure by de Jeu *et al.* [31], for the same molecule (figure 2). The curves are different from the Maier–Saupe prediction, falling off too rapidly just as the transition is approached, but can be fitted with equation (7), giving $Q^{**} = 0{\cdot}13$, $\kappa = 0{\cdot}13$, $\beta = 0{\cdot}32$ and $(T^{**} - T_{NI})/T_{NI} = 0{\cdot}18 \times 10^{-3}$. It is also noteworthy that the Maier–Saupe predictions for the ratio $\langle P_4\rangle/\langle P_2\rangle$ (figure 3) are higher than both the experimental values of Kohli *et al.* [32] and the predictions of the 50^3 Lebwohl–Lasher model which are in closer agreement with each other.

The quantification of short-range order in the pretransitional region ($T > T_{NI}$) has been followed through by the standard procedure of fitting the decay of the $G_2(r_{12})$ function to the Ornstein–Zernike expression to give the value of the coherence length ξ which increases as the temperature reduces towards T^*. The fit of the temperature dependence of the deduced coherence length with the de Gennes expression (9) gives an estimate of $(T_{NI} - T^*)/T_{NI}$ of $2{\cdot}9 \times 10^{-3}$ in reasonable accord with the experimental values which are in the range 3×10^{-3} to 4×10^{-3} [24, 25].

Below the transition temperature, the structure is really that of short-range correlations superimposed on the nematic long-range order. Figure 4 illustrates the decay of order with increasing pair correlation distance at values of T/T_{NI} of 0·9225, 0·9852 and 1. As the coherence length ξ was expected to reach infinity at T^* on cooling, the decreasing part of the plots of figure 4 were first fitted to (const/r_{12}), cf. equation (10). However the quality of the agreement was not satisfactory and a much better fit was obtained using the full Ornstein–Zernike form, which, with the long-range order component, $\langle P_2\rangle^2$, is:

$$G_2(r_{12}) = \frac{C}{r_{12}} \exp\left(\frac{-r_{12}}{\xi}\right) + \langle P_2\rangle^2. \qquad (17)$$

Fitting the model-generated data, the value of ξ appears to decrease with decreasing temperature below T^*, against a background of increasing $\langle P_2\rangle$. We should also like to point out that the largest value of ξ observed was 7·8 which was at the transition as defined by the

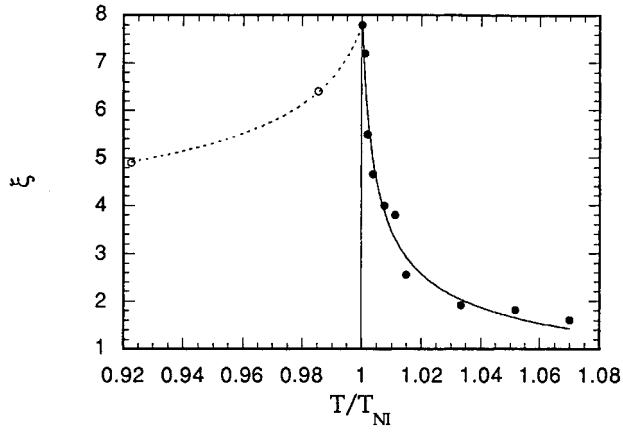

Figure 5. A plot of ξ against temperature spanning the transition region. The values of ξ were determined by fitting the Ornstein–Zernike equation (supplemented as in equation (17) for data below T_{NI}) to pair correlation data from the model. The plots are fitted with the de Gennes expression, equation (9), above T_{NI} and, for convenience, a similar symmetric expression below the transition.

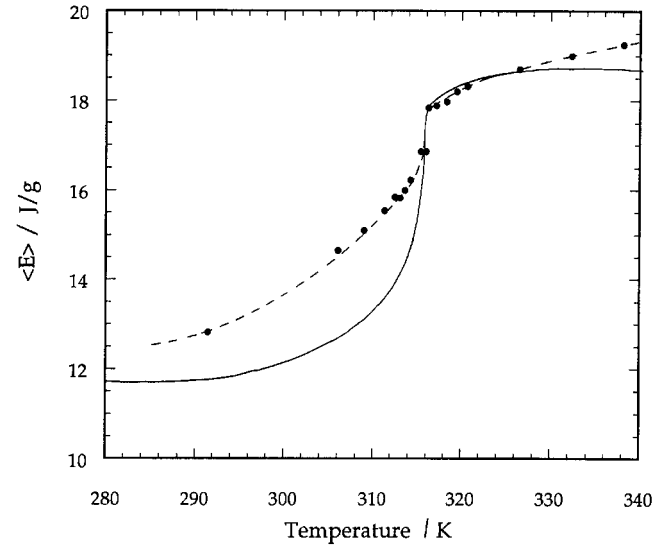

Figure 6. The local energy predicted by the model (dashed curve drawn through points) is compared with experimental data for enthalpy from [18] (full curve). The model data have been scaled to give a transition at 316 K, by scaling the value of A (§2.2) appropriately, and then converting into J g^{-1}. The two curves were set to coincide vertically at the point of maximum curvature.

discontinuity in the $\langle P_2 \rangle$ plot. Figure 5 is a plot of ξ and $\langle P_2 \rangle$ versus temperature across the transition range determined from the best fit to the Ornstein–Zernike form (17).

3.3. *Average energy as a function of temperature*

The total energy of the system as a function of temperature was measured by summing the individual cell energies for a given model and averaging over time. This energy is compared with calorimetric data from [18] in figure 6. The model data have been scaled to give a transition at 316 K, but scaling the value of A (see §2.2) appropriately, and then converting into J g^{-1}. The two curves were superimposed vertically at the enthalpy corresponding to the sharpest curvature of each plot, which can be identified with the transition point. It is apparent that in thermal terms the transition is broad, extending over several tens of degrees in either direction. A proportion of the energy change is however concentrated into a very small temperature interval, and this sharp feature has been taken as evidence for the weak first order character of the transition.

As a further check on the evidence for first order character of the transition, a plot was made of $(dH/dT)_{max}$ as a function of model volume, with the implication that the peak height would go to infinity with the model volume for first order behaviour. This plot, figure 7 (*a*), reproduces the data of Zhang and his best straight line which we have extrapolated to higher volumes. It would appear that the plot does genuinely linearize with the larger model size available now. The significant error band for the data point for the 50^3 model reflects the limited computer time allocated to this particular aspect of the current work. Figure 7 (*b*) is a plot to test the condition for the second order transition, namely that $(dH/dT)_{max}$ is proportional to $L^{\alpha/\nu}$, where α and ν are the critical exponents characterizing the singularities of specific heat [25]. These parameters have the values of 0·04 and 0·64, respectively. It is interesting to note that the data of Zhang are close to linear on this plot which would actually suggest a second order transition, perhaps also reflected in the curvature of his data in figure 7 (*b*). However, the addition of the datum for the 50^3 model does destroy the linearity and would thus appear to provide significant supporting evidence for the presence of first order character in the transition.

4. Microstructural description

4.1. *Microstructural diagrams*

One advantage of the LL model is that it is possible to examine the predicted orientational structure as a function of temperature. As with any model, especially one as large as 50^3, the problem is one of how best to display the results. Figure 8 shows the predicted structure of a section through the three dimensional model 10 K above the nematic–isotropic transition temperature of 298 K ($T = 1{\cdot}0332 T_{NI}$). The lines representing the orientation of the individual molecules shorten as the orientation rotates out of the plane. It is possible to identify regions of nematic type, referred to as nuclei;

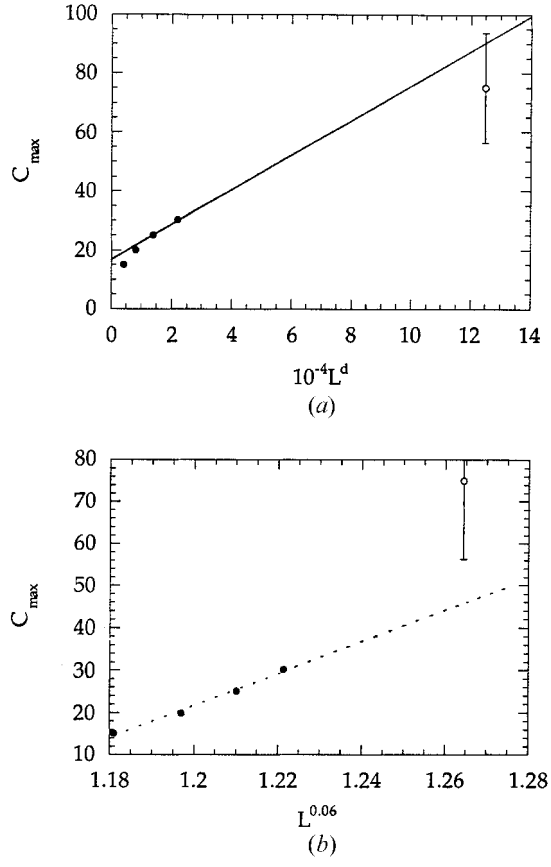

Figure 7. (*a*) Plot of the peak height of the (dH/dT) curve determined by Zhang and Zuckermann [12] (full points and the line fit) as a function of the volume of the model. The open circle was determined as a part of the current work with a 50^3 model. (*b*) Zhang and Zuckermann's data plotted against $L^{0.062}$. A linear plot would indicate a second order transition [12].

they have been outlined by eye. As the model runs with time, the nematic nuclei continually dissolve and reform. However, as the temperature is above the transition, the orientations of the nuclei are not correlated with each other, and there is no long-range orientational order. The question remains as to the best means of delineating the more ordered from the less well ordered regions.

4.2. *Distributions of local energy and their use in classifying more ordered and less ordered regions*

The distribution of the local energy will be an indicator of the presence of regions of different levels of order. Zhang and Zuckermann [12] have shown the existence of a double-well structure of the free energy appearing in a temperature range from about 0·3 K below to 0·3 K above the transition. This feature indicates that two states of order are present simultaneously in the bulk over this very narrow temperature range. However, the existence of short-range order in the isotropic phase is known to extend to much higher temperatures, at least ten degrees or more above T_{NI}, and these authors do not explore this range. We have therefore prepared energy distributions, $P(E)$, covering a wider temperature range.

In the case of a homogeneous state of order, $P(E)$ is a Gaussian function centred about the mean value E_0 of the internal energy at the temperature T. The value of E_0 is related to the global order parameter $\langle P_2 \rangle$ with expressions (11) and (13). The Gaussian is weighted by the Boltzmann factor, with a width proportional to the infinite lattice specific heat C [5]:

$$P(E) = \frac{A}{C^{1/2}} \exp\left(- \frac{(E - E_0)^2 L^d}{2kT^2 C} \right) \qquad (18)$$

and the distribution becomes progressively narrower as the temperature tends to 0 K.

In the LL model, the probability distribution is quite large in the isotropic state, since the molecules are free to rotate and to take any orientational position. Figure 9 shows the local energy distribution for the model with the directors representing the molecular axes oriented at random, fitted with a Gaussian. Close to the transition, and indeed at temperatures even greater than ± 10 K on either side of it, the calculated internal energy per site does not follow a normal distribution (cf. figure 10). In particular, the fact that the distribution at $1{\cdot}0332 T_{NI}$ is wider than for the random case is not realistic, as the width should decrease gradually with increasing order (decreasing temperature) towards zero width at 0 K. One way to fit the energy distributions in the transitional region is to use two Gaussian curves according to equation (18) which would correspond to the more ordered and less ordered regions of the structure. Such an approach is in line with the observation of a double peak in the global distribution at temperatures very close to the transition [12]. In general, the proximity of the ordered and disordered mean values, as well as the width of both Gaussians, result in a global distribution without double-peak structure. It should be emphasized that in discussing two discrete types of region, there is no implication of sharp borders, but instead a very diffuse interface between them. The fact that the two distributions overlap reflects the fact that there are low energy cells in the less ordered regions (as also there are in the isotropic state) and high energy cells as pockets of disorder in the more ordered regions.

The next step is actually to relate the energy distributions with spatial positions in the model. The objective is to identify two types of region, one more ordered than the other, and each with a Gaussian energy distribution. If each cell were ascribed to one of the two regions on the basis of its energy, with the discriminating energy being taken as the most probable (peak) energy, then the

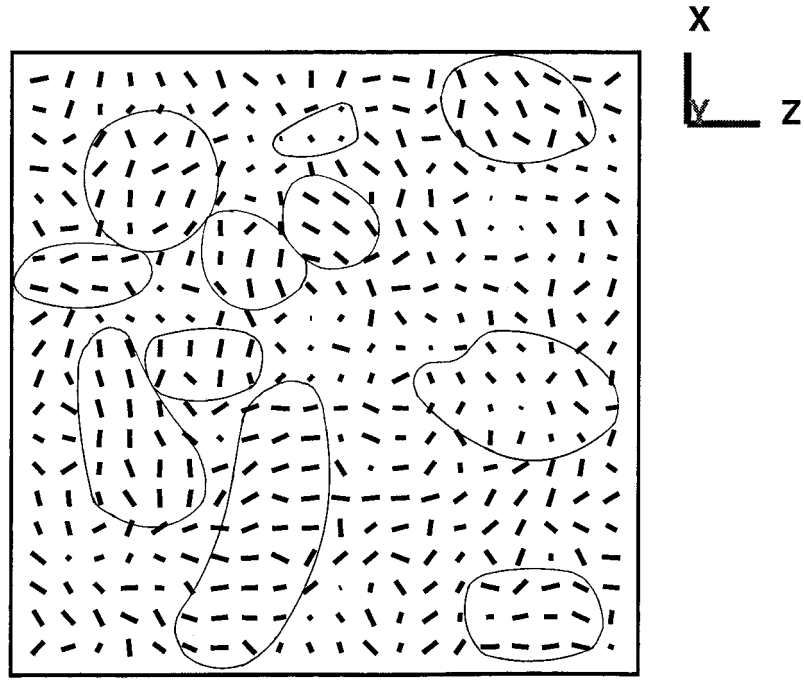

Figure 8. Part of a section of the model at $T = 1{\cdot}0332 T_{NI}$ with some nematic nuclei outlined. The director orientation out of the plane is indicated by the length of the line; a director normal to the section would appear as a point.

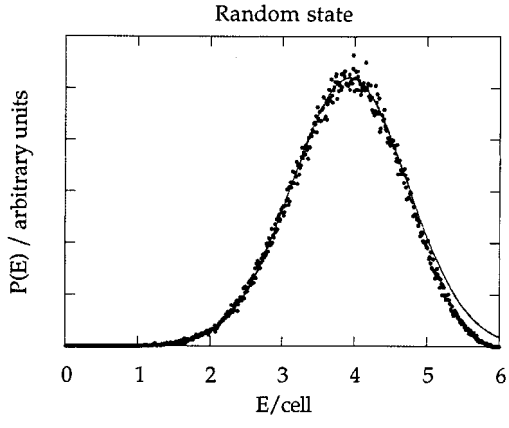

Figure 9. Energy probability distribution, $P(E)$, of a randomly oriented 50^3 array of directors. The model data have been fitted with a Gaussian distribution (solid line). The energies in this figure and those in the similar figures which follow are absolute energies, whereas $\langle E_{local} \rangle$ defined by equation (16) has a negative sign.

regions, while distinguishable, would be interpenetrating. Such a structural diagram would correspond to a simple vertical division of the overall distribution for $T = T_{NI}$, figure 11 (*a*). It is anticipated however that each of the regions will have its own Gaussian distribution, as illustrated in figure 11 (*b*).

In order to map the two types of region, each retaining its individual Gaussian distribution, the energies of the cells were smoothed spatially, so that isolated higher energy cells, or small groups of such cells within the more ordered regions, and *vice versa*, were assigned to their host phase. The smoothing was achieved by calculating the energy of each cell, also taking into account the average energy of the surrounding cells using:

$$E^i_{smooth} = \frac{1}{1+a+b} E^i_1 + \frac{a}{1+a+b} E^i_6 + \frac{b}{1+a+b} E^i_{20} \tag{19}$$

with E^i_1 the energy of cell i, E^i_6 the average energy over its 6 nearest neighbours and E^i_{20} the average energy over its 20 next nearest neighbours. The parameters a and b were set to 1 and 0·5, respectively. Not only the energy of the individual cells, but also the state of order around them, are thus taken into account. Cells with smoothed energies less than the most probable value of 2·70 were allocated to the more ordered regions, and those with greater energy to the less ordered. The two component energy distributions based on the actual (unsmoothed) energies obtained with this method (figure 12) are two Gaussians of equal magnitude. A degree of order can be determined for each type of region as that corresponding to their Gaussian mean values, and we find $\langle P_2 \rangle = 0{\cdot}50$ and $\langle P_2 \rangle = 0{\cdot}18$ for the more ordered and less ordered regions, respectively.

The same decomposition into two distinct types of region was performed at different temperatures, keeping the same values of E_{limit} and a and b. These distributions, shown in figure 13, illustrate the smooth change in the

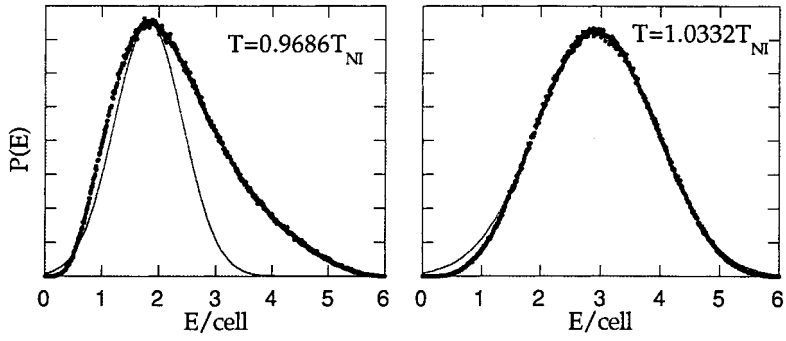

Figure 10. Energy distributions for two temperatures on either side of T_{NI}. It is apparent that there are difficulties in fitting a single Gaussian distribution. The lower temperature distribution is asymmetric, while the breadth of that at $1{\cdot}0332T_{NI}$ is wider than that for the random state model of figure 9.

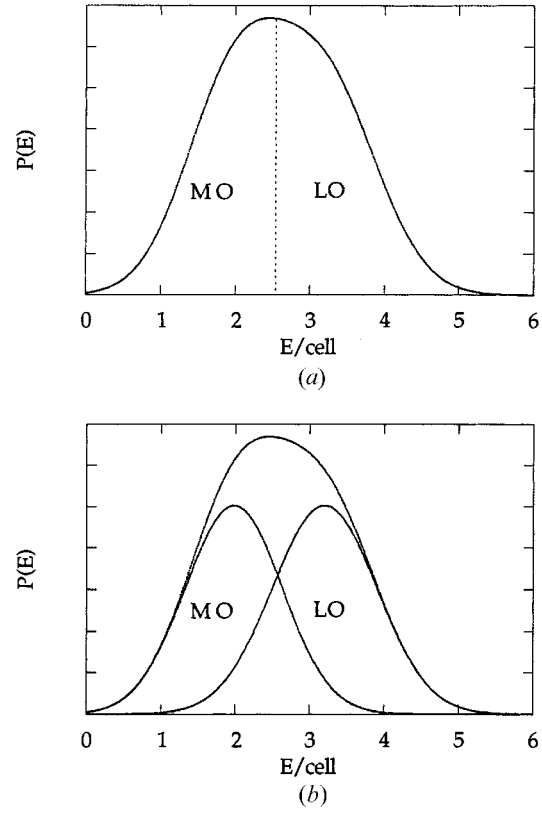

Figure 11. The energy distribution at T_{NI}: (*a*) divided at the energy of the peak of the distribution into areas representing more ordered and less ordered cells in relationship to their six nearest neighbours; (*b*) the division into two Gaussian peaks of equal area.

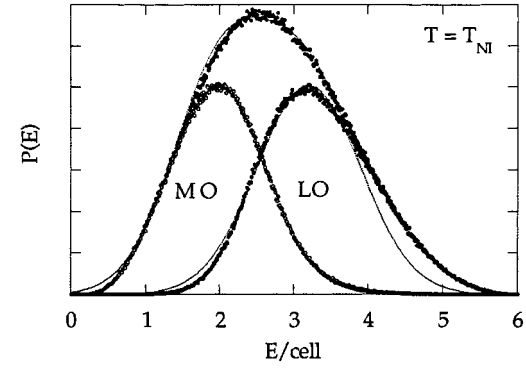

Figure 12. The energy distribution at T_{NI}, determined from the model, analysed into the two component Gaussians which represent the distribution of energies in the more ordered (MO) and less ordered (LO) regions.

relative amounts of the two regions across the transition range. Note how the relative peak heights change very rapidly with temperature at the transition itself. Figure 14 shows the peak height of the ordered component of the distribution as a function of reduced temperature. It is a measure of the volume fraction of the more ordered region. The order parameters within each of the two types of region do not change significantly over the temperature range investigated ($\pm 0{\cdot}0336T_{NI}$).

Where the component energy distributions have been developed in this way, the distribution of the more and less ordered regions in the model are available as a matter of course. The diagrams which constitute figure 15 are sections through the 50^3 model at three different temperatures. Figure 15(*a*) corresponds to $1{\cdot}0336T_{NI}$ ($T_{NI}+10$ K), figure 15(*b*) to T_{NI}, and figure 15(*c*) to $0{\cdot}9664T_{NI}$ ($T_{NI}-10$ K); each of the structures is decomposed into two figures, showing just the more ordered regions (top) and the less ordered regions (bottom). Figure 15(*d*) is another model of the structure at $1{\cdot}0336T_{NI}$, but in this case the nematic nuclei are depicted on a larger scale.

4.3. *Description of structure across the transition region*

Focusing first on figure 15(*a*), which shows the structure at $1{\cdot}0336T_{NI}$, the nematic nuclei are clearly apparent and occupy a significant volume fraction of the structure. It should be underlined again that structure is continually varying with time, and the top (more ordered)

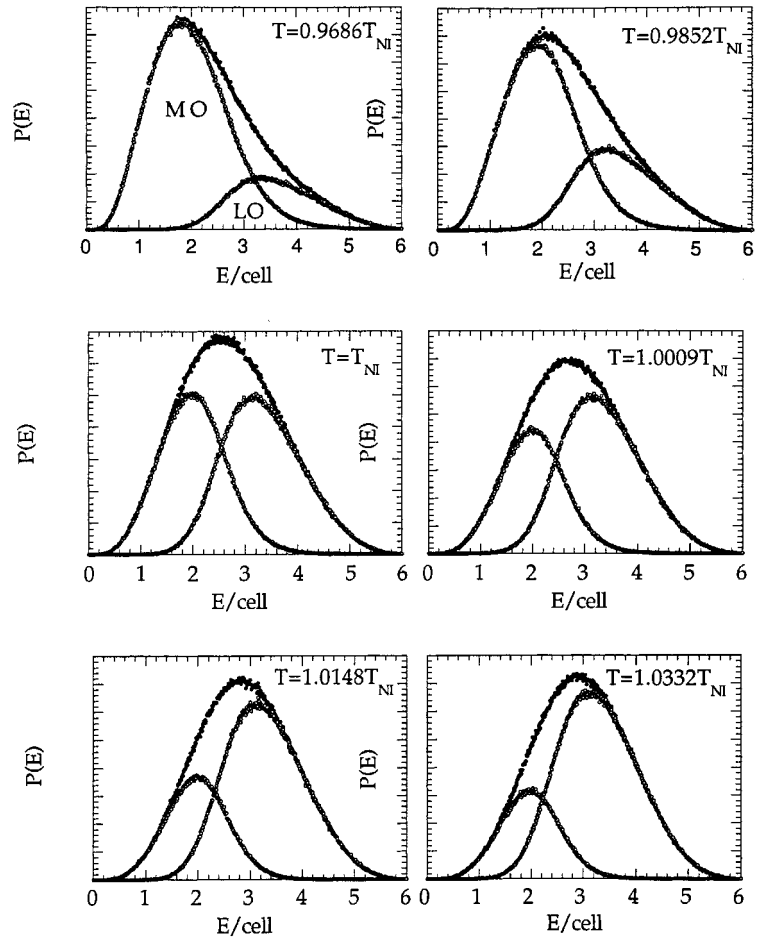

Figure 13. The more ordered and less ordered components of the distribution at different temperatures spanning the transition region. Note how the relative magnitudes of the two component distributions change rapidly in the immediate vicinity of the transition, while their peak positions and half width remain more or less constant, the less ordered (higher energy) distribution being wider than the more ordered one as anticipated.

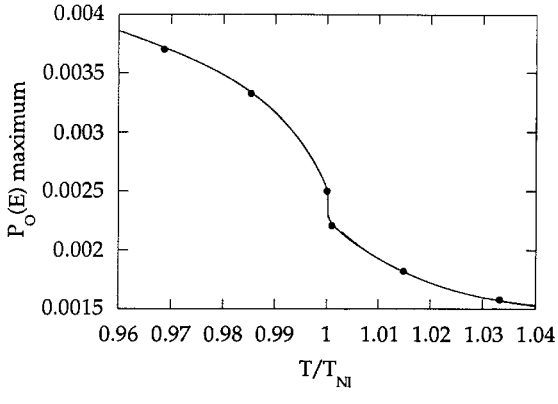

Figure 14. A plot of the amplitude of the ordered component distribution as a function of reduced temperature. Note how the amount of the more ordered regions reduces discontinuously close to the transition.

component of the figure shows the presence of orientation correlation within the nuclei, but the absence of orientational correlation between them. The more ordered regions are clearly the included 'phase', and the less ordered region the matrix.

Moving next to the structure at $0{\cdot}9664T_{NI}$, figure 15 (*c*), one sees a striking symmetry in appearance with figure 15 (*a*), the distribution of the less ordered regions being very similar to that of the more ordered regions at the equivalent temperature above the transition. The structure just below the transition consists of a continuous more ordered matrix region, which is the long-range orientational order defining the nematic state, and includes regions of significantly poorer order.

The actual transition itself, figure 15 (*b*), corresponds to the point at which the nematic nuclei present above T_{NI} percolate so that the more ordered regions now share a uniform orientation right across the model.

In this case, the common orientation happens to be close to the x axis so there is a predominance of blue coloured directors within the more ordered (top) section. Reduction in temperature below the transition leads to an increase in the volume fraction of the long-range ordered material with a corresponding reduction in the extent of the isolated, less well ordered regions as shown in figure 15 (c).

5. Discussion

5.1. *General*

The Lebwohl–Lasher model is remarkable in that while all chemical detail is reduced to a simple Hamiltonian based on $\sin^2(\Delta\theta)$, the model is nevertheless very successful in predicting much of the character of the nematic state in general, and the nematic–isotropic transition in particular.

There is evidence that the structure can, in the region of T_{NI}, be represented by two regions, one less ordered, the other more ordered. With decreasing temperature in the isotropic phase the nematic nuclei, which are randomly distributed in both time and space, increase in volume fraction. On cooling through the transition itself, these nuclei appear to percolate. Hence, while there is a comparatively gradual increase in local order summed throughout the structure, as indicated by the considerable width of both recorded and simulated enthalpic maxima, there is a critical point at which P_2 for an infinite model and the presence of long-range (i.e. percolating) orientational order, as would be indicated by birefringence, both increase discontinuously from zero. Below the transition, the more ordered region is continuous throughout the specimen, even though it contains significant but isolated regions of disordered material, and it can be considered as the matrix phase. The order parameter within the more ordered region at the transition temperature is estimated to be $\langle P_2 \rangle = 0{\cdot}5$.

5.2. *The relevance of percolation theory*

It is useful to consider the degree to which the observed behaviour of the model in the region of the transition is consistent with simple percolation theory.

For a site percolation model on a three dimensional simple cubic lattice, the fraction of sites occupied at percolation, (the percolation threshold) will be 0·31. However, this simple analysis assumes several factors which need to be examined in assessing its applicability to the nematic–isotropic transition. Firstly, it is possible to view mean field approaches in terms of infinite dimensionality (which can be rationalized in terms of a Bethe lattice, or tree) where the percolation threshold will be 0·5. More significantly, it is necessary to relate the fraction of unoccupied sites to the thermal randomization of the orientations of random sites. It has been suggested, [33] p. 152, that the fraction of sites 'occupied' can be expressed as $1-\exp(-\Delta H/kT)$. Furthermore, the Hamiltonian of equation (13) means that the probability of randomization of the orientation ascribed to a cell with respect to its immediate surroundings depends on the orientational order of those surroundings.

These factors mean that the percolation approach to the transition, while being useful as a descriptor, is not straight-forward. Indeed, according to Coniglio *et al.* [34] who worked with the three dimensional Ising model, the percolation point (appearance of the first infinite cluster) and the critical point (appearance of magnetization, in the case of the ferromagnet studied in this reference) do not coincide in the 3 dimensions case. However, probably the closest developments have been in the context of the percolation approach to the Heisenberg model of the paramagnetic–ferromagnetic transition, where magnetization states are able to assume any orientation rather than being restricted to up and down states as in the Ising model. Here the divisions of the structure into regions of different degrees of order are seen to be the basic thermal excitations of the system, just as phonons are those of solids [35]. Yet, percolation theory is not yet exact for ferromagnetic systems, nor, by implication, for nematics. The fact that the ordered regions effectively have a surface energy, means that the treatment of the percolation threshold is in doubt for a start.

What is more, it is possible that the percolation relevant to the critical point of the phase transformation is between the nuclei themselves. However, even this picture is complicated as the nuclei are of all conceivable orientations and the percolating phase, by definition, is of one orientation. The fact that the volume fraction of the more ordered material at the transition is seen from the model to be of the order of 50% must be contrasted with the critical volume fraction for continuum percolation which, in three dimensions, has the value of 0·16 and is remarkably insensitive to the structure of the packing, whether ordered or not (see, for example, [33] p. 186). Is it possible that one third of the growing nuclei are able to recognize each other as having sufficiently similar orientations so that they can clamp and amalgamate?

While the question must remain open, it is worth noting that in the formation of a liquid crystalline phase, there is a mechanism by which two impinging nuclei of similar although not identical orientation can merge. Where two nuclei approach within the site pair correlation distance, the region between them can be described as a wall, of a type represented by the two limiting cases of Bloch and Neel walls in ferromagnetics. Now, this wall can lower its energy by increasing its width via

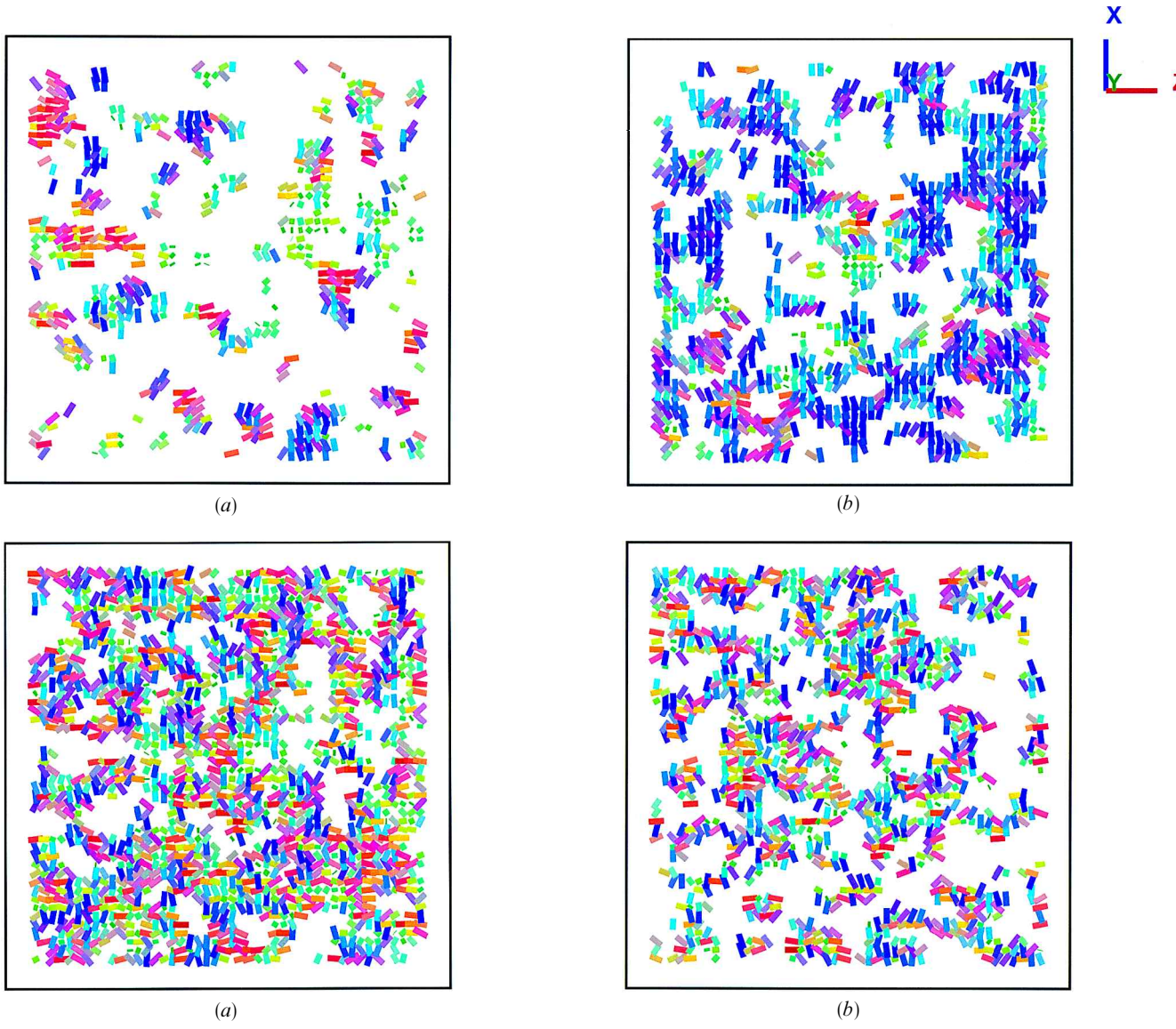

Figure 15. Sections through the 50^3 model at three different temperatures. In each case (*a*, *b* and *c*) the upper diagram represents the more ordered phase, the lower diagram represents the more ordered phase, the lower diagram the less ordered, both being complementary. The orientations are represented by the orientation of the director line on the page and its length: in addition the orientation is colour coded. (*a*) $T = 1{\cdot}0332T_{NI}$; (*b*) $T = T_{NI}$; (*c*) $T = 0{\cdot}9686T_{NI}$; (*d*) is an enlarged section of a model prepared under the same conditions as that in (*a*) showing the nematic nuclei.

elastic relaxation, which will lead to a more generalized elastic distortion in the combined entity. Such behaviour can be observed in regions of the more ordered, just percolating phase, seen in figure 15 (*b*). It is also possible that the energetics of the process can contribute to the transient, first order character of the transition. The removal of the distorted boundary material between the adjacent nuclei will itself contribute to a rapid increase (with temperature) of the volume of the more ordered regions as demonstrated by the data of figure 14.

6. Conclusions

A 50^3 Lebwohl–Lasher model has been successfully run. The size of the model, which is 5^3 larger than the average coherence length of short range order in the isotropic phase, has allowed a direct description of behaviour of a nematic material. The model gives values of $\langle P_2 \rangle$ which agree well with experiment, and the Ornstein–Zernike fit of the angular pair correlation coefficient gives a value of the stability limit of the isotropic phase $T^* = 0{\cdot}997T_{NI}$ also in good agreement

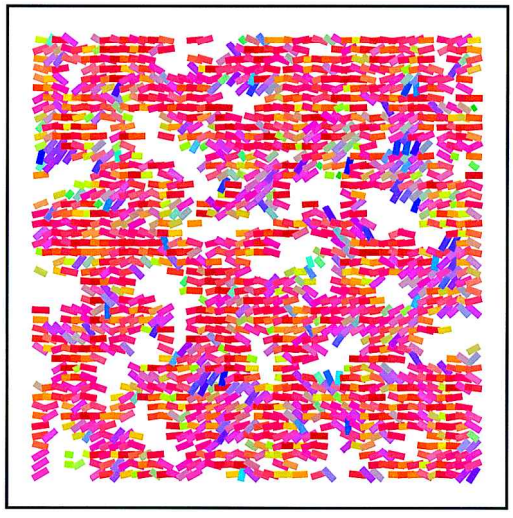

(c)

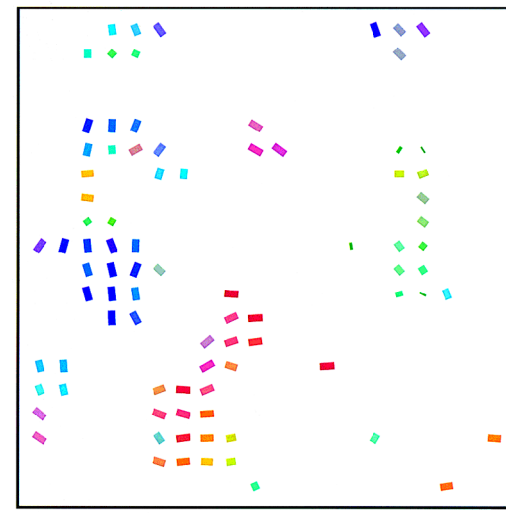

(d)

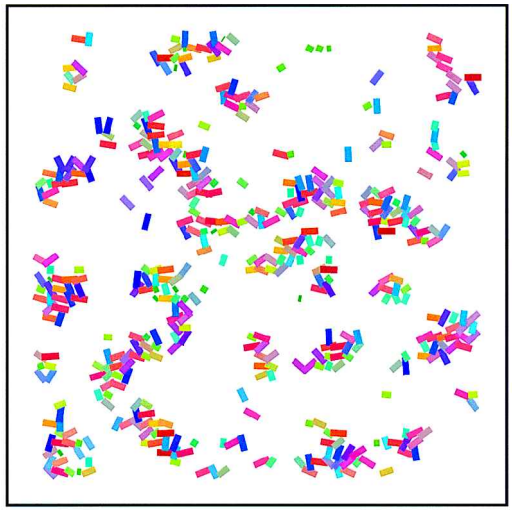

(c)

Figure 15. (*Cont.*)

with experiment. These agreements engender confidence that the model is working properly.

The model has been applied primarily to predict microstructures in the region of T_{NI} as follows. Above T_{NI}, isolated nuclei of more ordered (nematic) regions occur, which are not orientationally correlated with each other; T_{NI} corresponds to the point where the nematic nuclei percolate to produce the nematic superdomain. Below T_{NI} the structure consists of the long-range ordered nematic matrix phase containing isolated regions of considerably disordered material which shrink with further reduction in temperature.

The parallels between the observed transition (figure 15) and the precepts of percolation theory are compelling. However, the application of this theory to the nematic–isotropic transition, as indeed to the equivalent ferromagnetic–paramagnetic one, is far from straightforward. This line of pursuit is likely to be highly rewarding.

This research was funded by a research training fellowship at the research centre of the Commission of the European Communities, under the Human Capital and Mobility Programme. The authors wish to acknowledge helpful discussions with Professor Philip Taylor, Professor Tim Slukin, John Hobdell and David Hoyle, and the support of Marc Lavine with particular aspects of the computational programme.

References

[1] Lebwhol, P. A., and Lasher, G., 1972, *Phys. Rev. A*, **6,** 426.
[2] Humphries, R. L., and Luckhurst, G. R., 1982, *Proc. R. Soc. Lond.*, **A382,** 307.
[3] Luckhurst, G. R., and Simpson, P., 1983, *Chem. Phys. Lett.*, **95,** 149.
[4] Shukla, P., and Sluckin, T. J., 1985, *J. Phys. A*, **18,** 93.
[5] Challa, M. S. S., Landau, D. P., and Binder, K., 1986, *Phys. Rev. B*, **34,** 1841.
[6] Fabbri, U., and Zannoni, C., 1986, *Mol. Phys.*, **58,** 763.
[7] Zannoni, C., 1986, *J. Chem. Phys.*, **84,** 424.
[8] Romano, S., 1988, *Liq. Cryst.*, **3,** 323.
[9] Chiccoli, C., Pasini, P., and Zannoni, C., 1988, *Liq. Cryst.*, **3,** 363.
[10] Chiccoli, C., Pasini, P., and Zannoni, C., 1988, *Physica*, **148A,** 298.
[11] Lee, J., and Kosterlitz, J. M., 1991, *Phys. Rev. B*, **43,** 3265.
[12] Zhang, Z., and Zuckermann, M. J., 1993, *Mol. Phys.*, **80,** 1195.
[13] Zhang, Z., Mouritsen, O. G., Otnes, K., Riste, T., and Zuckermann, M. J., 1993, *Phys. Rev. Lett.*, **70,** 1834.
[14] Cleaver, D. J., and Allen, M. P., 1993, *Mol. Phys.*, **80,** 253.
[15] Chiccoli, C., Pasini, P., and Semeria, F., 1993, *Phys. Lett. A*, **176,** 428.
[16] Greeff, C. W., and Lee, M. A., 1994, *Phys. Rev. E*, **49,** 3225.
[17] Maier, W., and Saupe, A., 1960, *Z. Naturforsch.*, **15A,** 287.
[18] Richardson, M. J., 1993, *Thermochim. Acta*, **229,** 1.
[19] Luckhurst, G. R., 1979, in *The Molecular Physics of Liquid Crystals*, edited by G. R. Luckhurst and G. W. Gray, (London: Academic Press) p. 85.
[20] McColl, J. R., and Shih, C. S., 1972, *Phys. Rev. Lett.*, **29,** 85.
[21] de Gennes, P. G., 1969, *Phys. Lett.*, **30A,** 454.
[22] de Gennes, P. G., 1971, *Mol. Cryst. Liq. Cryst.*, **12,** 193.
[23] de Gennes, P. G., 1993, *Long- and Short-Range Order in Nematics*, 2nd Edn (Clarendon Press) pp. 76–91.
[24] Gramsbergen, E. F., Longa, L., and De Jeu, W. H., 1986, *Phys. Rep.*, **135,** 195.
[25] Anisimov, M. A., 1988, *Mol. Cryst. Liq. Cryst.*, **162A,** 1.
[26] Biscarini, F., Zannoni, C., Chiccoli, C., and Pasini, P., 1991, *Mol. Phys.*, **73,** 439.
[27] Chiccoli, C., Pasini, P., Semeria, F., Sluckin, T. J., and Zannoni, C., 1995, *J. de Physique II*, **5,** 427.
[28] Ferrenberg, A. M., and Swendsen, R. H., 1988, *Phys. Rev. Lett.*, **61,** 2635.
[29] Bedford, S. E. and Windle, A. H., 1993, *Liq. Cryst.*, **15,** 31.
[30] Zannoni, C., 1979, in *The Molecular Physics of Liquid Crystals*, edited by G. R. Luckhurst and G. W. Gray (London: Academic Press), Chap. 3, pp. 51–83.
[31] De Jeu, W. H., and Claassen, W. A. P., 1978, *J. Chem. Phys.*, **68,** 102.
[32] Kohli, M., Otnes, K., Pynn, R., and Riste, T., 1976, *Z. Physik B*, **24,** 147.
[33] Zallen, R., 1983, *The Physics of Amorphous Solids* (London and New York: Wiley).
[34] Coniglio, A., Nappi, C. R., Peruggi, F., and Russo, L. 1977, *J. Phys. A.*, **10,** 205.
[35] Stauffer, D., and Aharony, A., 1994, in *Introduction to Percolation Theory* (London and Bristol [PA]: Taylor and Francis), p. 142.